ASTRONOMY & ASTROPHYSICS
SUPPLEMENT SERIES

Astron. Astrophys. Suppl. Ser. **130**, 119–132 (1998)

Deep Hα survey of the Milky Way

IV. The $l = 301°$ to $l = 324°$ area*

D. Russeil, Y.M. Georgelin, P. Amram, J.L. Gach, Y.P. Georgelin, and M. Marcelin

Observatoire de Marseille, 2 place Le Verrier, F-13248 Marseille Cedex 04, France

Received July 17; accepted November 21, 1997

Abstract. The detailed velocity field of the ionized hydrogen has been observed between $l = 301°$ and $l = 324°$ as part of an Hα Survey of the southern Milky Way. Analysis of the Hα profiles shows six different velocity components. These Hα observations, combined with multiwavelength and stellar data, are used to find the most probable distances of the different gas layers.

Key words: interstellar medium: HII regions — Galaxy: structure

1. Introduction

The study of the large scale spiral structure of our Galaxy requires us to identify and find the distances of the large star-forming complexes defining the arms. In order to do this we use the main tracers of star formation, particularly HII regions and their exciting stars and the molecular clouds where they were born.

The Hα Survey of the Milky Way, being undertaken at La Silla (ESO) by the Marseille Observatory, allows us to probe the discrete HII regions, and the more diffuse Hα emission, in the direction of the southern Galactic plane. Such a survey is necessary in order to resolve the distance ambiguity problem in the radio domain for lines of sight at $l > 270°$ (two distances are then possible for a given velocity). Also, it allows us to observe the diffuse interstellar medium widely described by Reynolds (1979, 1984, 1987). Closely linked to HII regions from the kinematics point of view, the diffuse Hα emission is sometimes the unique tracer of the spiral structure (Russeil 1997).

The Hα emission of HII regions is the link between molecular clouds and the young hot stars, so it allows the determination of the stellar distance to the molecular clouds. Unfortunately, because of the interstellar absorption, the distances of stars can be estimated only for the nearest ones. Moreover, spectrophotometric data of southern early type stars are not numerous, so often kinematic information alone is available. Hα detection is then essential to help in chosing between the two allowed kinematic distances.

Since the complexes are active star forming zones, they frequently exhibit small scale gas velocity variations from place to place ("champagne" flows, internal motions, etc). In order to determine their systemic velocities we have to quantify these variations gathering the multiwavelength kinematic information of the different sources forming a complex. Then we determine the distance using a rotation model.

The present study covers the Galactic longitude and latitude ranges $l = 301°$ to $324°$ and $b = -2°$ to $2°$. Here we present only the data, further interpretation in terms of spiral structure being required to put this zone into relation with the adjacent ones. Georgelin et al. (1987, 1988) have already examined the HII regions in this area, but the new observations from our Hα survey of the southern Galactic plane clearly show the necessity of this more detailed study.

The radio continuum at 5 GHz (Haynes et al. 1978) in this longitude range exhibits either radio sources in close groups ($l \sim 306.5°$ and $l \sim 317°$) or larger groups ($l \sim 311°$ $-313°$) or over an extended emission area ($l \sim 307.6°$, $l \sim 300°$, $304°$ and $l \sim 322°$ $-324°$). In any one group, it is not rare that sources exhibit different velocities. Indeed, for such a line of sight several arms are going to be intercepted and a superposition of emissions located at different distances is usually expected, in which case it is important to distinguish the different velocity groups and to place them in a coherent spiral structure. In Sect. 2 of this paper we will present observations and data reduction. Section 3 is devoted to the study of the kinematical informations between $l = 301°$ and $324°$. The stellar information and distance estimations will be also

Send offprint requests to: D. Russeil

* Based on observations collected at the European Southern Observatory.

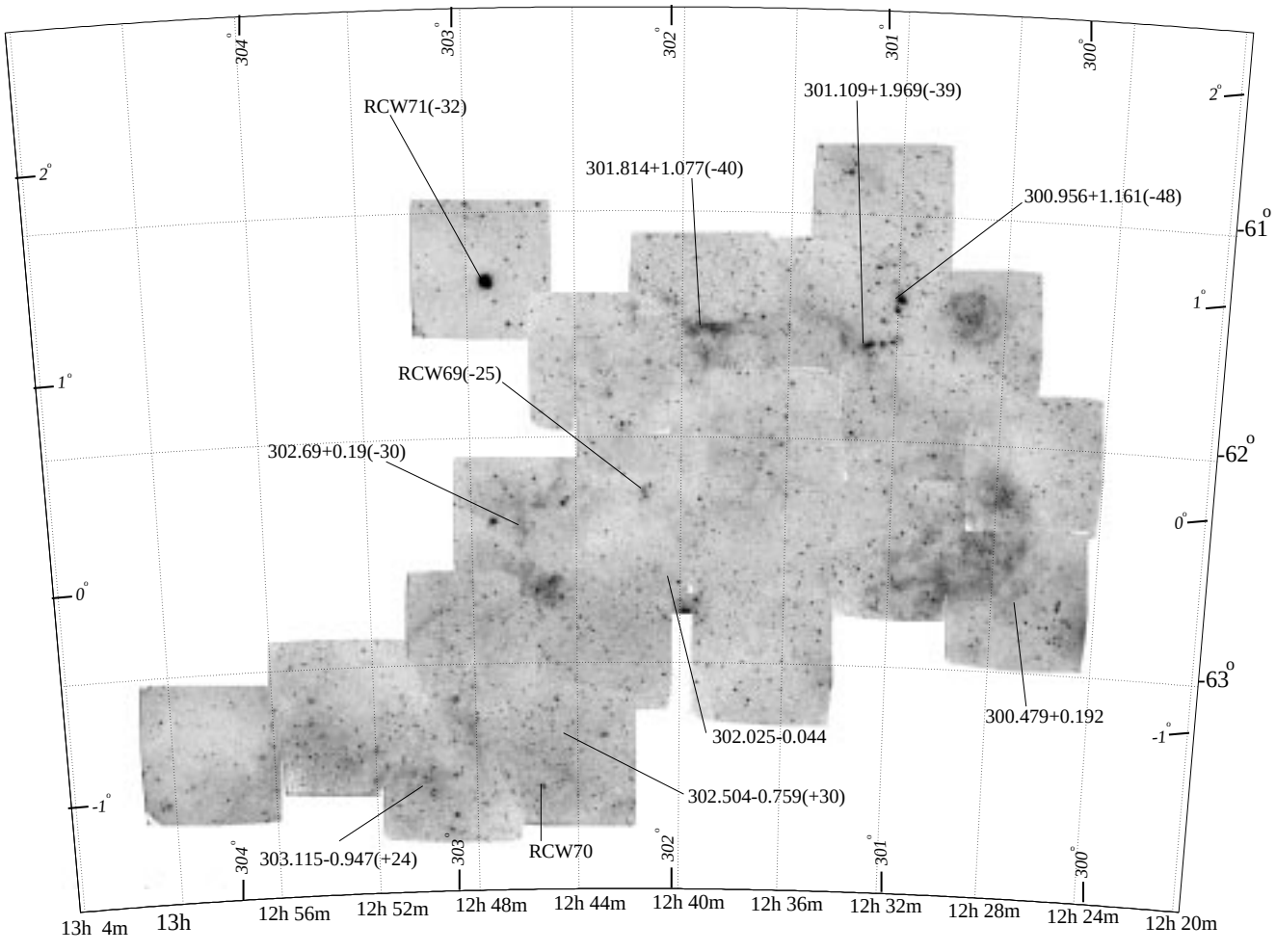

Fig. 1. a) Hα mosaic of the observed fields in the 301° zone. Each image is obtained by adding λ maps over the whole free spectral range, flat fielding and then correcting for distortion. This is equivalent to a photograph obtained through a filter with a 10 Å bandwidth. The positions of radio sources and HII regions are shown with the corresponding Hα velocity values, when observed

discussed in this part of the paper. The conclusion is given in Sect. 4.

2. Observations

The Hα observations presented here were made at La Silla with a small telescope (36 cm diameter) equipped with a scanning Fabry-Perot interferometer and a photon counting camera (le Coarer et al. 1992). The data cubes (x, y, λ) obtained have a spatial resolution of $9'' \times 9''$ (total size of each field = $38' \times 38'$) and a spectral resolution depending on the interference order of the Fabry-Perot: $\sim$5 km s^{-1} for order 2604 and $\sim$ 16 km s^{-1} for order 796.

The data reduction method is described in Georgelin et al. (1994). The interference filter, centered at 6562 Å and with FWHM 11 Å, unfortunately transmits not only the Hα nebular emission but also two well identified night-sky lines: geocoronal Hα (λ_0 = 6562.8 Å) and OH (λ_0 = 6568.8 Å).

In order to decompose the observed profiles into elementary components, the night-sky line and the nebular ones will be respectively modeled by a pure instrumental profile, and an instrumental profile convolved with a gaussian.

The decomposition of high emission zones allows us to identify the different components encountered along the line of sight. However, the decomposition becomes trickier when the emission zones are fainter, even if each component generally has about the same velocity across the entire field.

The actual fields observed in Hα were selected on the basis of large scale photographic data (Georgelin & Georgelin 1970) and the 5 GHz radio emission survey (Haynes et al. 1978). They include the regions previously studied by Georgelin et al. (1987, 1988); most of these were observed with a fixed order Fabry-Perot interferometer, the others with a scanning Fabry-Perot interferometer with a very small field (diameter $\sim$12′). We note that for some regions previously observed we do not find

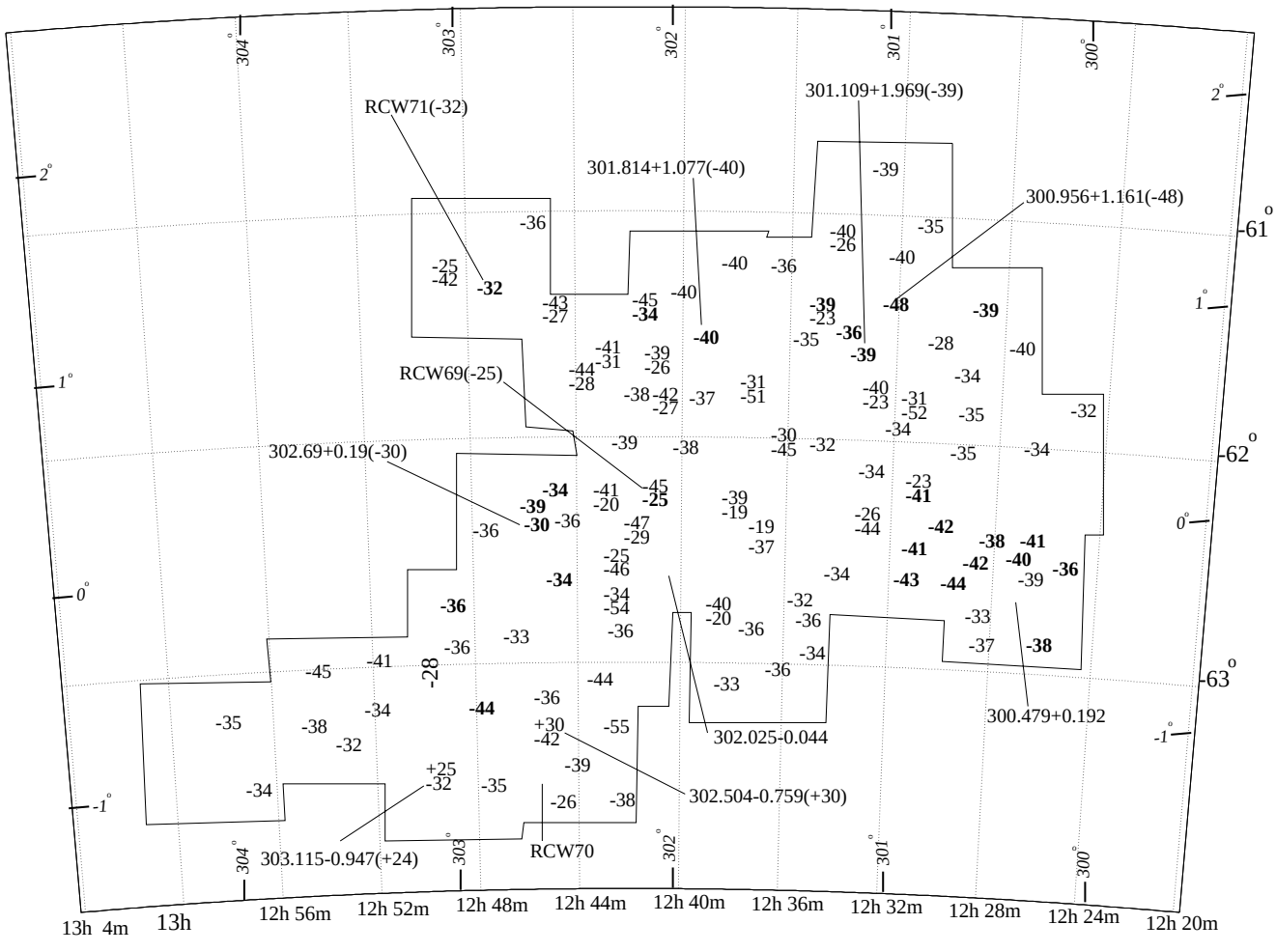

Fig. 1. b) Spatial distribution of velocity components in the 301° area. Only the non-local components are indicated. Note that the velocities of the diffuse Hα emission, as well as those of the discrete HII regions, are shown at the points of measurements. Bold letters correspond to Hα emission patches in the mosaic. Very closely placed numbers represent multiple components at one point of measurement

exactly the same velocity. It is obvious that the old observations made with a fixed Fabry-Perot did not allow any profile decomposition, thus preventing night-sky lines subtraction and faint component separation, so the velocities corresponded to a complex blend.

3. Results

The total longitude interval has been divided into five zones centered near longitudes 301°, 305°, 308°, 313° and 320°, corresponding roughly to the more or less compact concentrations seen from the morphology of the radio continuum emission.

The main results are summed up in Figs. 1 to 5. Figures 1 and 2 show the mosaic of the 301° and 305° zones, accompanied by the velocity maps of all the components, except the local one, corresponding to diffuse emission or discrete HII regions. Figures 3 to 5 show the fields of zones from 308° to 320° with the velocity information plotted directly on them.

Note that in the following discussion the kinematic distances are calculated from the mean Galactic rotation curve of Brand & Blitz (1993) with $R_\odot = 8.5$ kpc and $\theta_0 = 220$ km s^{-1} for $V_{\rm lsr} < 0$ and a flat curve, at 220 km s^{-1}, for $V_{\rm lsr} > 0$.

For each zone, we selected stars with spectral type between O and B3 from the literature. Stellar distances were determined from the spectrophotometric data (UBV, Hβ), when available, using the absolute magnitude spectral type calibration of Schmidt Kaler (1983) and the extinction relation $A_v = 3.2E(B-V)$. For a small number of HII regions, we were able to identify the exciting stars. These regions and their distances are discussed individually below. The star clusters were selected from the Lynga (1987) catalogue. The adopted distance is generally the one given by Lynga, except when a more recent reference is available.

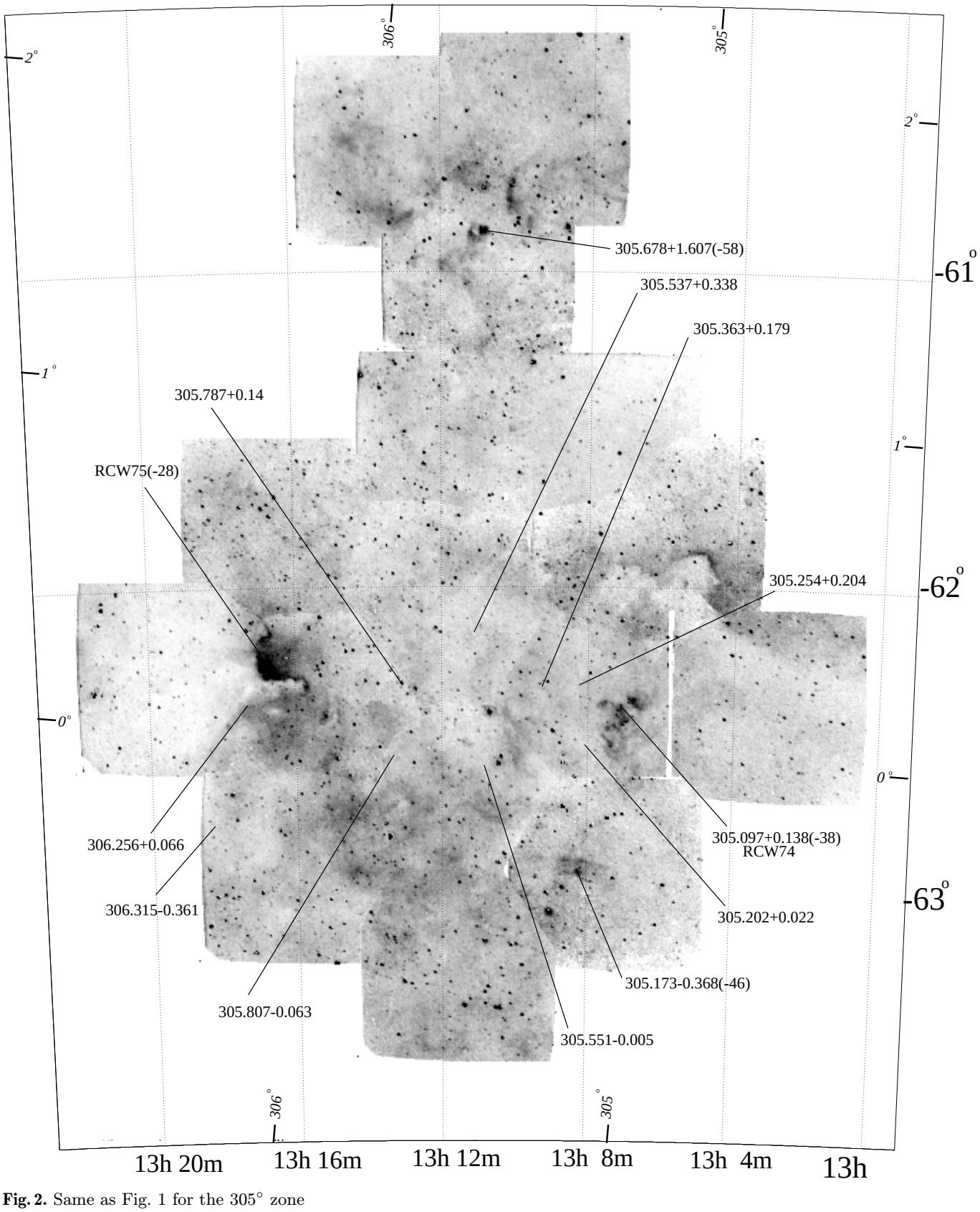

Fig. 2. Same as Fig. 1 for the 305° zone

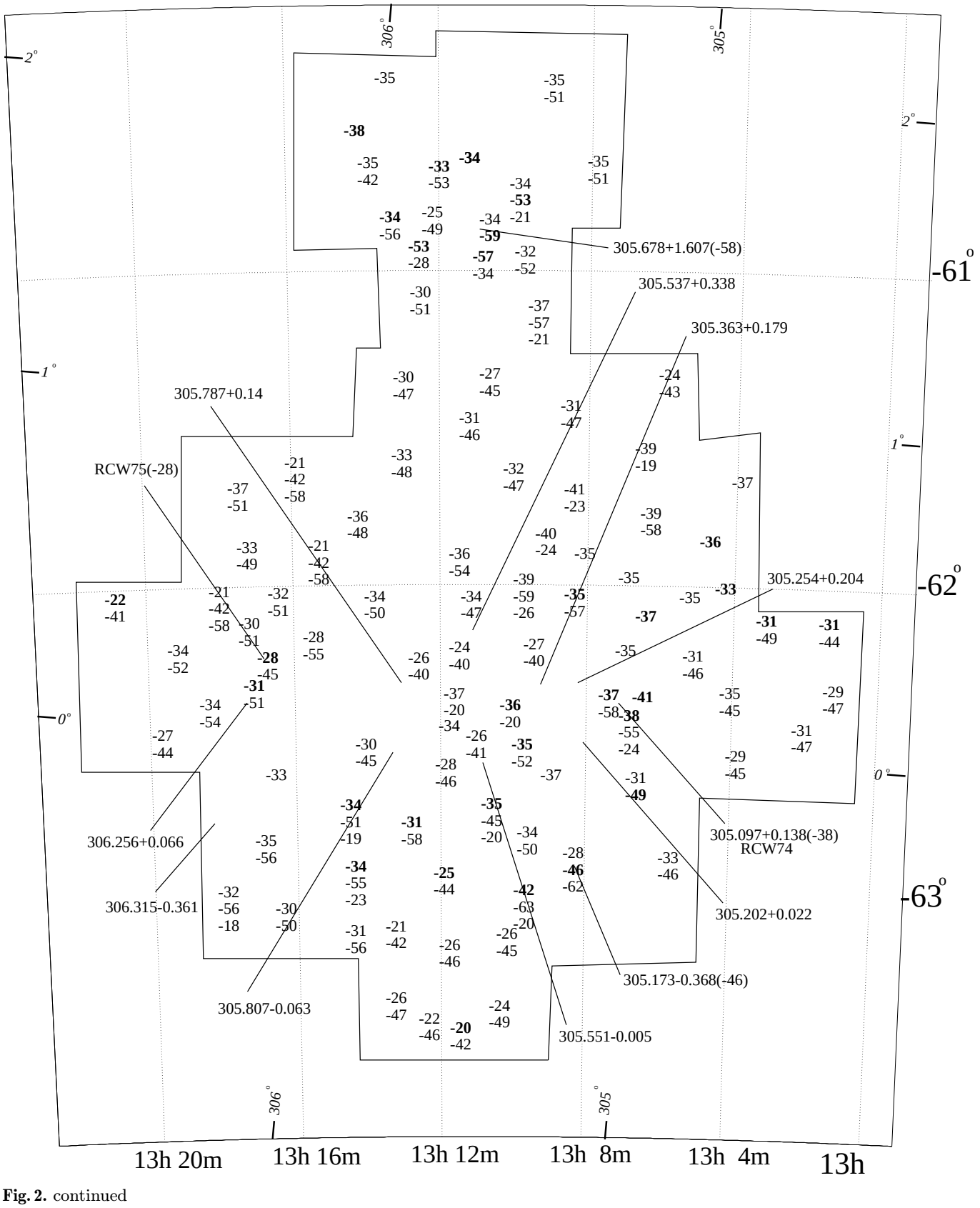

Fig. 2. continued

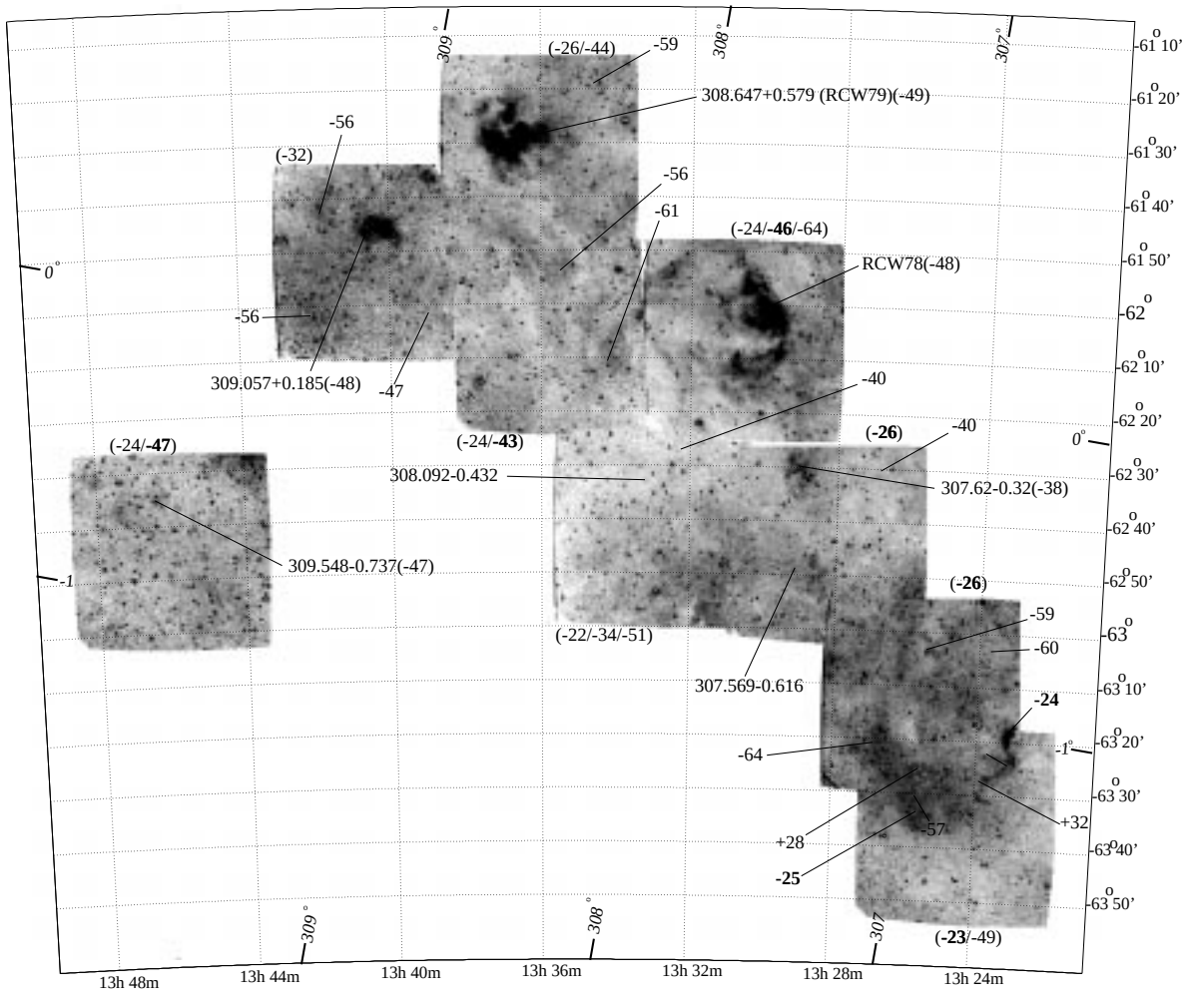

Fig. 3. Hα mosaic of the observed fields in the 308° zone. Each image is obtained by adding λ maps over the whole free spectral range, flat fielding and then correcting for distortion. This is equivalent to a photograph obtained through a filter with a 10 Å bandwidth. The positions of radio sources and HII regions are shown with the corresponding Hα velocity values, when observed. Velocities indicated in parentheses are for diffuse components present all over the field. The other velocities are for the points indicated. Only the non-local components are indicated. Bold letters correspond to Hα emission patches in the mosaic

Table 1 summarizes the radial velocities of discrete HII regions and areas bright in Hα, for the total longitude range. These sources are grouped into complexes from the kinematic and distance information:

- *Column 1:* Identification of the source. Radio continuum sources are identified by their l, b coordinates and Hα sources by their RCW number (Rodgers et al. 1960) or their α, δ coordinates. Molecular clouds are indicated by CO preceding their l, b coordinates.
- *Column 2:* Our Hα $V_{\rm lsr}$ velocity.
- *Column 3:* H 109α line velocity from Caswell & Haynes (1987) or other authors when the reference is specified.
- *Column 4:* CO velocity (rounded to nearest km s^{-1}) and reference. Some data come from unpublished observations recently carried out at the SEST radiotelescope in La Silla (Russeil & Castets 1998).
- *Column 5:* Absorption line velocity and reference.
- *Column 6:* Deduced systemic velocity for the group.
- *Column 7:* Stellar distance.
- *Column 8:* Adopted distance.

3.1. Details concerning each zone

We now give the main conclusions that can be drawn from the stellar and kinematic data in each zone in order to determine the distance of each velocity component. These components are separated into discrete HII regions and diffuse emitting layers.

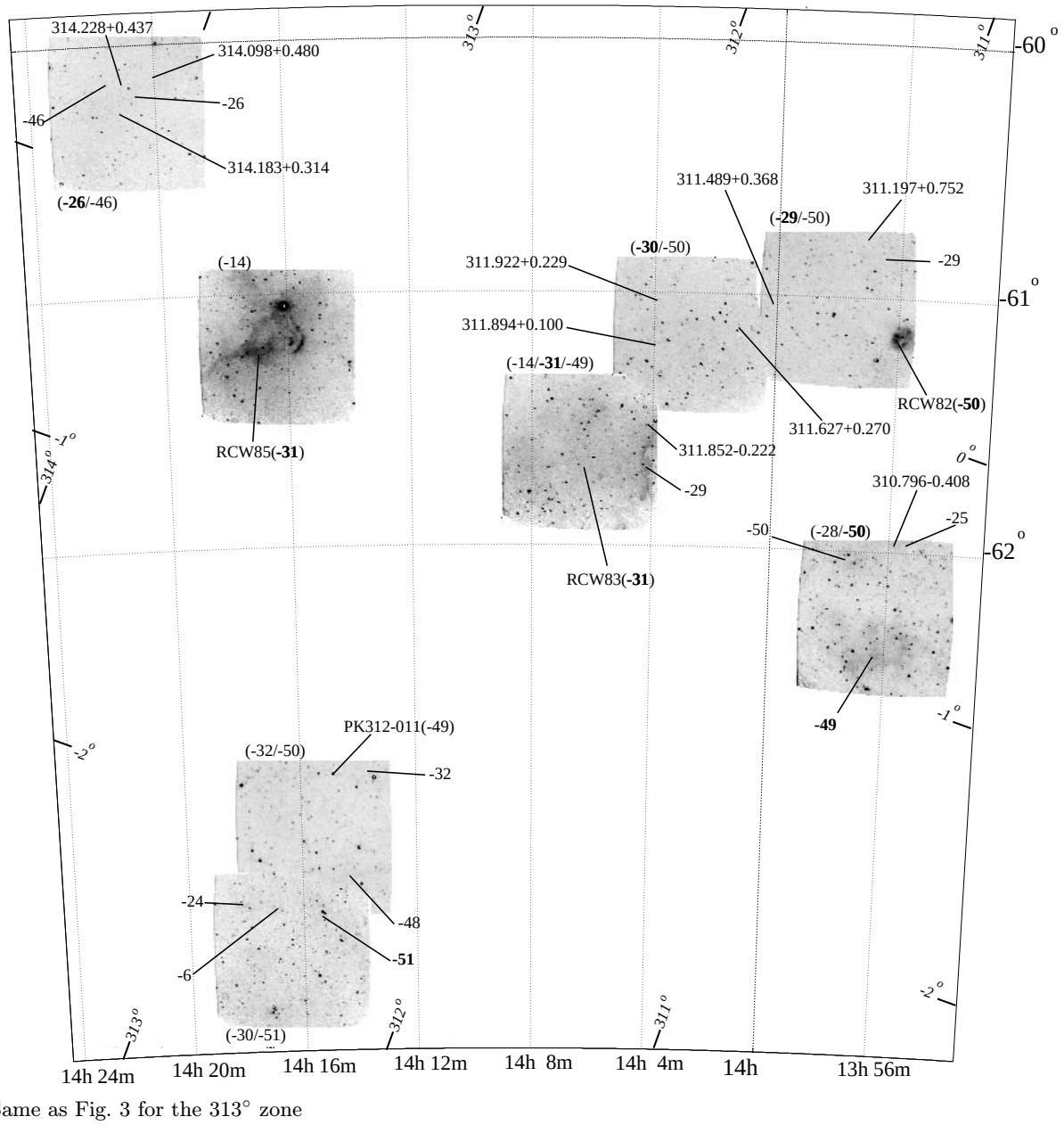

Fig. 4. Same as Fig. 3 for the 313° zone

3.1.1. 301° zone

One diffuse component, widely distributed over the observed area, with no visible small-scale structure, is well detected in Hα. Its velocity is between −7.4 and 0.4 km s^{-1}. It is probably linked to the Coalsack. Indeed, this dark cloud lies at $l = 300°$ to 306.9°, $b = -4.3°$ to +2.4° and has a CO velocity between −2 and −6 km s^{-1} (Nyman et al. 1989). Seidensticker & Schmidt Kaler (1989) give its distance as 180 pc from stellar spectrophotometry. We call this diffuse emision layer the local layer.

In addition to this component several others are identified (Figs. 1a and 1b).

A second group, with mean velocity −33 km s^{-1}, includes several Hα patches and the HII regions RCW 69 and RCW 71. The diffuse emission extends over a large velocity range (−19 to −35 km s^{-1}). It is important to note that in this direction ($l = 301°$) the tangent point radial velocity is −33 km s^{-1} ($d_{\rm kin} \sim 4.4$ kpc). However Brand (1986) proposes for RCW 69 a stellar distance of 2.13 kpc, and RCW 71, excited by HD 311999, has a distance of 2.11 kpc. We conclude that this group can be put at 2.0 kpc, especially since the star clusters NGC 4439 (1.6 kpc), NGC 4463 (1.18 kpc) and NGC 4755 (2.1 kpc) as well as the early type field stars (mean ∼ 1.7 kpc) have similar distances.

The third group, with a mean velocity of −40 km s^{-1}, includes bright Hα patches at $12^{\rm h}30^{\rm m}$, $-62°30'$, as well as the group of radio sources located farther north and exhibiting slightly more negative mean velocities. However,

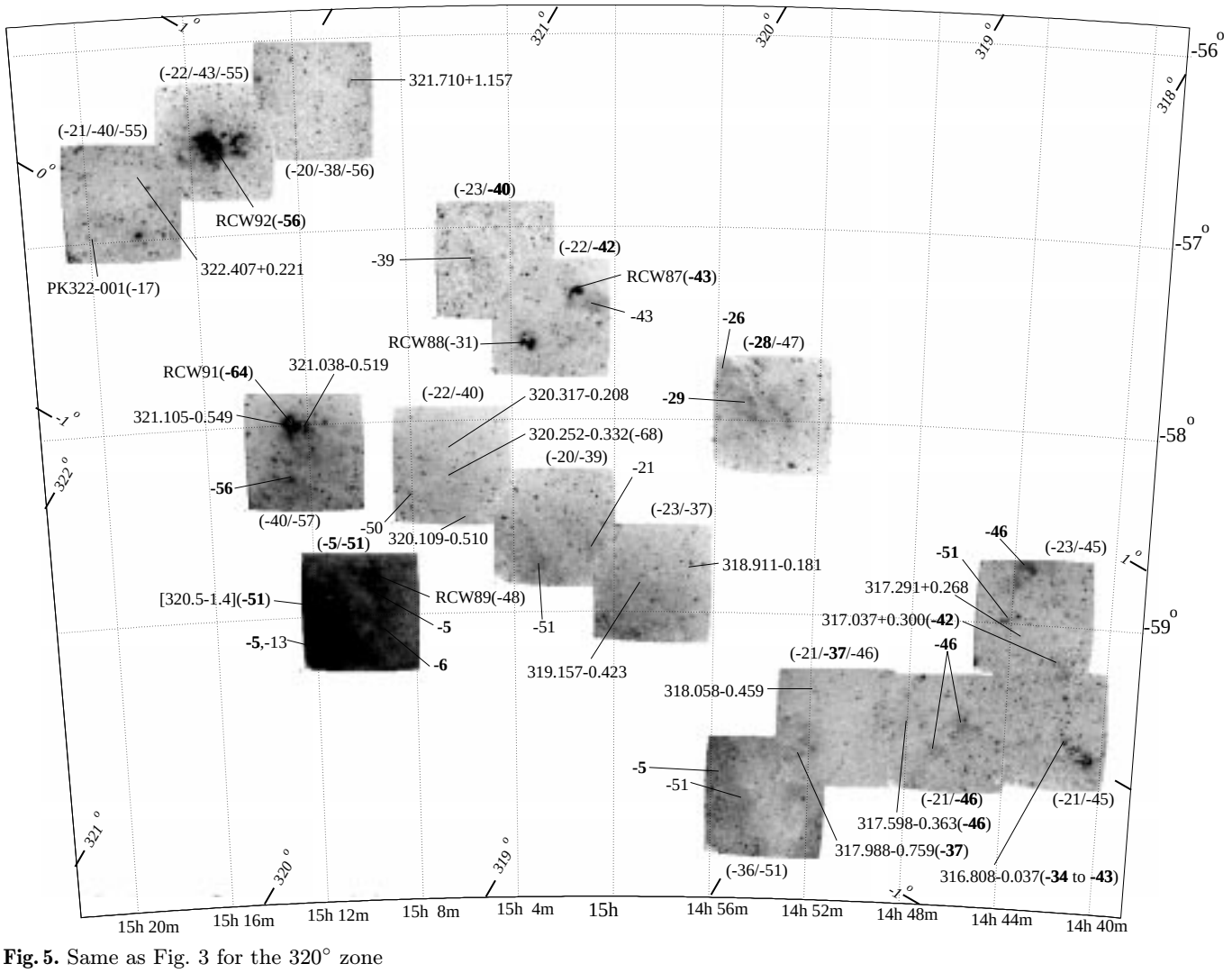

Fig. 5. Same as Fig. 3 for the 320° zone

velocities around −40 km s^{-1} are outside of the range of velocities predicted by the model (thus indicating departures from pure circular rotation). Moreover, no stellar distance information is available for this group. We assign to this group the distance of the tangential point which comes closest ($d_{\rm kin}$ = 4.4 kpc, $V_{\rm lsr}$ = −33.3 km s^{-1}) to the measured velocity. Such a velocity deviation was previously observed at l = 298° (Russeil 1997) with an Hα component of the same velocity. The associated HII region RCW 64 has a stellar distance of 5.4 kpc.

Finally, some distant radio sources with positive velocities are detected in Hα. Already discussed by le Coarer et al. (1992), this group has a mean velocity of +26 km s^{-1}, for which the rotation model gives the unique distance of 11.5 kpc. These sources can be linked to two giant molecular clouds – clouds 31 and 32 discussed by Grabelsky et al. (1988) – with velocities + 31 and +29 km s^{-1}. Detection of these sources indicates inhomogeneous absorption in this direction, where the Coalsack's influence is still present. Similarly, at l = 298° (Russeil 1997), sources with velocities of the same order have already been observed, delineating the far part of the Carina arm. The same conclusion can be applied to the new sources detected here.

3.1.2. 305° zone

This Galactic direction was studied by Georgelin et al. (1988) using previous Fabry-Perot Hα observations. They concluded that the line of sight in this direction, located at the eastern edge of the Coalsack, intercepts numerous radio continuum sources which form a large radio complex (1°6 ×1°5), whose only visible Hα counterpart is the HII region RCW 74. With velocities between −40 and −50 km s^{-1}, RCW74's distance is between 3.5 and 4.0 kpc according to Danks et al. (1984). RCW 75 has a clearly different velocity, it is located in front of this large complex, hence independent of it.

The new observations, with a more detailed coverage of this zone, confirm the main conclusions of Georgelin et al. (1988).

Again, the proximity of the Coalsack can easily explain the nearby diffuse Hα emission, widely distributed over the observed area, with velocities between 0 and -8 km s^{-1}. Another diffuse component, with velocities between -18 and -23 km s^{-1}, is observed in some places, particularly in the southern field of the mosaic, suggesting a link with the large HII region (not visible in our images) centered at $l = 306°$, $b = -2°$ which has the same velocity (Georgelin et al. 1988). We note that the radio source $306.315 - 0.36$ is not seen directly in Hα, but in the corresponding $38'$ field it is necessary to add a component at -18 km s^{-1} in order to fit the observed Hα profile. Indeed, this source appears to be located behind the edge of a strongly absorbing area. Comparison of the profiles observed inside and outside of this area shows the intensity variation of this -18 km s^{-1} component.

Two other diffuse components, around -33 and -45 km s^{-1}, are found simultaneously in most of the Hα profiles. However, most of the Hα patches correspond to the -33 km s^{-1} component. The velocity of the HII region RCW 75 is -28 km s^{-1}. Thus the diffuse components between -26 and -34 km s^{-1} are probably associated with RCW 75 which, being excited by the star cluster Stock 16, is located at 2.3 kpc.

Most of the radio continuum sources probably belong to a complex of average velocity -38 km s^{-1}, although some of them show extreme velocities (e.g. -46 km s^{-1} for $305.173 - 0.368$) revealing strong internal motions. Moreover, the CO observations show two distinct components at about -38 and -43 km s^{-1}; but the more intense line is at -38 km s^{-1} for the majority of our SEST observations. Additional CO components, observed at around -28 km s^{-1}, are due to the foreground molecular cloud associated with RCW75. Despite the fact that only RCW 74 and $305.173-0.368$ are Hα emitting regions, we choose the near kinematic distance for this complex. This conclusion is favoured by the detection of diffuse Hα emission at -45 km s^{-1}. Such detection would be unlikely at the far kinematic distance.

Finally, a Hα component with velocity between -63 and -53 km s^{-1} also appears in some very localized places (see Figs. 2a and 2b). Only one radio source (305.678+1.607) exhibits a comparable velocity (-58 km s^{-1}); this seems to be its radio counterpart. On CO maps (Bronfman et al. 1989) one notes emission from a small independant molecular cloud with velocities around -52 km s^{-1} for $b > 1°$ and $305°5 < l < 306°$, in good agreement with our Hα observations. This velocity is more negative than the tangential point velocity by 10 km s^{-1}, so we adopt the tangential point distance. The kinematic complexity in this direction may be explained by the presence of the possible SNR detected at 2.4 GHz by Duncan et al. (1995). This source appears to be a semi circular arc tracing the northern part of the 4° diameter circle centered at $l = 304°$ and $b = 2°$. By continuity, the south-east portion of this structure would go through the group detected in Hα at -52 km s^{-1}, and could thus explain this anomalous velocity.

The other diffuse components, with velocities between -51 and -63 km s^{-1}, are found near HII regions with large internal motions, such as RCW 74 and $305.173 - 0.368$. This latter region has two main parts with different velocities (-43 and -54 km s^{-1}). Integrating the Hα profiles over all of $305.173 - 0.368$ gives a mean velocity of -46 km s^{-1}, which we adopt as its systemic velocity.

3.1.3. 308° zone

Again the local diffuse component ($V_{\rm lsr} = -1$ to -9 km s^{-1}) is present. A second diffuse component with $V_{\rm lsr} = -22$ to -29 km s^{-1} is also found over all of the observed area. This component is stronger in the southern part of the mosaic: a small, bright HII region ($13^{\rm h}23^{\rm m}.8 - 63°23'$) and an extended patch ($13^{\rm h}25^{\rm m}.6$ $-63°31'$), with similar Hα velocities, are clearly visible (Fig. 3). In the patch, positive velocity components are observed also. These correspond to small filamentary arcs which are clearly visible in the appropriate velocity maps. Furthermore, Duncan et al. (1995) detect a large ring centered near $l = 303°5$, $b = 0°$with a 9° diameter. Morphologically, the large HII region (centered at $l = 306°$ and $b = -2°$), more than 3° in diameter, already mentioned in Sect. 3.2, seems to be linked to this SNR. So the positive velocity components may be either local substructures, or due to the SNR expansion, rather than being due to very distant emission as indicated by the rotation law.

It is interesting to note that the number of star clusters near the galactic plane is higher towards longitude 308° than at smaller longitudes, which is consistent with the greater strength of the diffuse component. These star clusters, NGC 5138 (1800 pc), Hogg 16 (2130 pc), Collinder 271 (1600 pc), Collinder 272 (2900 pc), NGC 5168 (1400 pc), Trumpler 21 (1100 pc) and NGC 5281 (1300 pc), give a mean distance for this group of 1700 pc.

Two other groups of velocities of HII regions are also observed, at -48 km s^{-1} and -36 km s^{-1}. A very inhomogeneous diffuse emission with similar velocities is observed. We can divide the large velocity range of the diffuse emission into two groups: one with velocity between -30 km s^{-1} and -40 km s^{-1}, which seems to be associated to the -36 km s^{-1} group, and the other one with velocity between -40 and -70 km s^{-1} which can be associated with the -48 km s^{-1} group. Indeed around RCW 78 we find velocity components between -60 and -70 km s^{-1} which are superimposed on the brighter component at -48 km s^{-1}. This may be due to internal motions, as suggested by the peculiar structure of this region.

The stellar distance of RCW 78 (4.2 kpc) is in agreement with the kinematic distances of its associated regions. So we choose this distance for the full group. Concerning the -36 km s^{-1} group, no stellar information at all is available, so we opt for the near kinematic distance of 2.8 kpc.

3.1.4. 313° zone

In this direction the Hα emission exhibits three principal velocity components. As observed in the neighbouring areas, the first component (with $V_{\rm lsr}$ between -2 and -5 km s^{-1}) is the local diffuse emission showing a smooth distribution, without any condensation.

The second component (with $V_{\rm lsr}$ between -24 km s^{-1} and -31 km s^{-1}) is a diffuse emission, distributed over the whole zone, to which the HII regions RCW 83 and RCW 85 (with $V_{\rm lsr} = -31$ km s^{-1}) can be associated. In fact, RCW83 and RCW85 are probably two parts of a single HII region, mainly excited by the star HD 124314. This spectroscopic binary, with spectral type O6V, is located at 1500 pc. Six star clusters at about the same distance are also linked to this layer: Lynga 1 (1.0 kpc), Lynga 2 (1.1 kpc), Hogg 17 (1.6 kpc), Trumpler 22 (1.6 kpc), NGC 5617 (1.6 kpc) and NGC 5606 (1.8 kpc). No radio sources with known H109α line velocities are linked to this Hα group. But one can see in Table 1 that several molecular clouds and HI absorption lines with similar velocity components (-23 to -27 km s^{-1}) are found towards more distant HII regions.

The third component involves velocities between -46 and -52 km s^{-1}. This layer shows weak diffuse emission, over all the observed zone, with some more structured areas of emission. On the mosaic one can see for instance RCW 82, Hα $13^{\rm h}56\overset{\rm m}{.}0 - 62°23'$ and Hα $13^{\rm h}57\overset{\rm m}{.}5$ $-62°02'$. Among these individual regions, only RCW 82 has a radio counterpart. Note, also, a region with velocity -49 km s^{-1} located at $14^{\rm h}06^{\rm m}$, $-61°30'$ which is likely due to the SNR $312.4 - 0.4$ ($V_{\rm H_2CO} = -49$ km s^{-1}) located behind RCW $83 - 85$ (HII regions of the preceding group). The mean distance of the stars farther than 2 kpc is 3.4 ± 0.9 kpc; this can be used as an estimate of the distance of this Hα layer.

There are no detectable Hα counterparts of the radio sources which define other complexes identified in the table. This fact is in agreement with the choice of the far kinematic distance. In particular, the group at -47 km s^{-1} is not seen in Hα, which is consistent with its greater distance.

3.1.5. 320° zone

As in the preceding regions the local layer, with velocities between -2 and -6 km s^{-1}, is widely detected. It is linked here with the molecular cloud $317 - 4$ ($5° \times 4°$; $V_{\rm lsr} = -6$ km s^{-1}; Dame et al. 1987), located at 170 pc.

This faint diffuse Hα emission at -4 km s^{-1} was previously mentioned by Georgelin et al. (1987). However, since an HII region covering several degrees at $l \sim 320°$ $b \sim -2°$ (the brightest part of which was called BBW 28802 by Bok et al. 1955), of the same velocity, was centered on O stars situated at about 1 kpc, Georgelin et al. assumed that this diffuse emission lays in the nearest part of the Sagittarius Carina arm. In the same paper, the Hα counterparts of radio sources $316.8 - 0.0$ and $317.0 + 0.3$ were observed and linked with the other spiral tracers. The better coverage of this area obtained from the new observations allows us to clarify the kinematics and hence the distance of the objects.

With the same velocity as the local layer, BBW 28802 seems now to be simply a brighter part of this layer. If this is the case it is not excited by the central stars HD 135591 (O7.5 III) and HD 135240 (spectroscopic binary O7.5III) situated at the mean distance of 1.2 kpc. In the field at $15^{\rm h}10^{\rm m}$ $-59°$ in Fig. 5 this velocity component may be interpreted either as a single component showing a velocity gradient from -5 to -10 km s^{-1} or as two components at -5 and -13 km s^{-1} with varying relative intensities. Recently two more fields were observed at $15^{\rm h}20^{\rm m}$, $-61°$, nearer to the O stars (these fields are not shown in Fig. 5). In addition to the quite faint -47 km s^{-1} emission, which is probably linked to Hα $[320.5 - 1.4]$ and RCW 89, one finds a particularly wide (30 km s^{-1}) line which can be decomposed into two lines, at -4 and -13 km s^{-1}. In this case the two stars would excite an HII region with velocity -13 km s^{-1}, different from the local diffuse emission, and located behind it at 1.2 kpc. This hypothesis is corroborated by the HI absorption lines at -4 and -12 km s^{-1} found toward RCW 89 (see Table 1) and by the NaI absorption lines present in the spectra of the two O stars, respectively $V_{\rm lsr} = -24.2, -15.2$ and -1.0 and $-16.3, -10.9, -1.8$ and 4.1 km s^{-1} (Crawford 1992).

On longitude–velocity CO maps (Bronfman et al. 1989) one sees a cloud over a large range in Galactic latitude, at longitudes greater than 317.75°, with velocities around -20 km s^{-1}. This cloud may be connected with the diffuse Hα which we observe over the whole zone, with velocities between -20 km s^{-1} and -23 km s^{-1}. Note that there is no corresponding radio source. The young stellar content consists of 24 stars with distances less than 2 kpc (1.34 kpc $\pm$ 0.33) and the star cluster Hogg 18 which is located at 1.0 kpc.

It is not clear that RCW 88, at -31 km s^{-1}, and the brightest emission observed at $14^{\rm h}55^{\rm m}$ $-58°$ with velocity -28 km s^{-1}, is connected with this group. If so they have particular motions; if not they are farther away.

All the other structured regions seen in Fig. 5 belong to more distant layers. They exhibit a mixture of components with a large velocity range: -36 to -51 km s^{-1}. Several molecular lines exist, implying a probable

Table 1. $V_{\rm lsr}$ radial velocities of HII region complexes only

Object name	Hα km s^{-1}	H 109α km s^{-1}	CO km s^{-1}	Abs km s^{-1}	$V_{\rm syst}$ km s^{-1}	$d_\star$ kpc	$d_{\rm adopted}$ kpc
300.479−0.192		26	9/27/32 (1)				
302.504−0.749	30	31	28 (1)				
303.115−0.947	24	26	4/21/24 (1)		+26		11.5
Hα12$^{\rm h}$50$^{\rm m}$.0−63°31′							
Hα12$^{\rm h}$52$^{\rm m}$.1−63°25′	22						
CO 300.3−0.2			31 (3)				
CO 301.8+0.0			24 (3)				
CO 302.3−0.7			32 (3)				
CO 303.9−0.4			29 (3)				
300.956+1.161	−48	−47		−43 (2)			
= RCW 65			−43 (15)				
301.109+0.969	−39	−42	−40/−35 (1)	−41 (2)			
= RCW 66			−42/−37 (15)				
301.814+1.077	−40	−42	−42 (1)				
= RCW 68							
Hα12$^{\rm h}$40$^{\rm m}$.6−61°23′	−40						
Hα12$^{\rm h}$39$^{\rm m}$.2−61°38′	−38						
Hα12$^{\rm h}$27$^{\rm m}$.1−62°37′	−40				−40		4.4
Hα12$^{\rm h}$27$^{\rm m}$.8−62°14′	−39						
Hα12$^{\rm h}$27$^{\rm m}$.5−62°31′	−40						
Hα12$^{\rm h}$28$^{\rm m}$.8−62°26′	−38						
Hα12$^{\rm h}$29$^{\rm m}$.9−62°38′	−42						
Hα12$^{\rm h}$30$^{\rm m}$.6−62°24′	−42						
Hα12$^{\rm h}$32$^{\rm m}$.5−62°44′	−39						
Hα12$^{\rm h}$31$^{\rm m}$.7−62°38′	−44						
Hα12$^{\rm h}$29$^{\rm m}$.2−61°26′	−39		−33 (1)				
302.69+0.19	−30	−33	−40 (1)				
RCW 71	−32	−32	−3 (1) −38/−30/−3 (15)			2.1	
302.025−0.044		−27	−36/−34 (1)	−35 (2)	−34		2.1
Hα12$^{\rm h}$45$^{\rm m}$.6−62°39′	−33						
Hα12$^{\rm h}$46$^{\rm m}$.1−62°24′	−30						
Hα12$^{\rm h}$45$^{\rm m}$.5−62°17′	−34						
RCW69	−25		−45/−37/−23 (15)		−24	2.1	2.1
305.678+1.607	−58	−58	−51/−46/−29 (1)				
Hα13$^{\rm h}$10$^{\rm m}$.3−60°46′	−53						
Hα13$^{\rm h}$11$^{\rm m}$.5−60°58′	−57				−52		4.9
Hα13$^{\rm h}$12$^{\rm m}$.7−60°57′	−53						
RCW 74	−38	−38	−37/−29/−25/−4 (1)				
305.097+0.138				−43/−2 (4)			
305.173−0.368	−46	−45	−24 (1)				
305.202+0.022		−40	−46/−35 (5)	−44/−34 (4) −45/−37 (6)			
				−45/−34 (6) −46/−33 (12)			
305.254+0.204		−39	−38/4 (5) −39 (9) −37 (14)	−38/−5 (4) −40 (6) −35 (6)			
305.363+0.179		−38	−39/−14/−3 (5)	−35/−4 (4) −41/−35 (6)	−38		3.5
			−40/−35 (14) −38 (9)	−39/−35 (6) −40 (12)			
				−45/−33/−22/−3 (11)			
305.537−0.338		−39	−38/−16 (1)	−38/−16 (4) −39 (2)			
305.551−0.005		−45	−84/−38/−3 (5)	−37/−31/−3 (4) −31 (6)			
305.787+0.14		−43	−43/−36/−32 (1)	−36 (2)			
305.807−0.063		−30	−41/−35 (1)	−40 (2)			
306.256+0.066	−34	−37	−28 (14)				
Hα13$^{\rm h}$14$^{\rm m}$.7−62°42′	−34						
Hα13$^{\rm h}$14$^{\rm m}$.4−62°53′	−34						
Hα13$^{\rm h}$10$^{\rm m}$.8−62°41′	−33						
Hα13$^{\rm h}$10$^{\rm m}$.0−62°31′	−33				−28		2.3
Hα13$^{\rm h}$10$^{\rm m}$.2−60°45′	−34						
Hα13$^{\rm h}$13$^{\rm m}$.5−61°0′	−34						
Hα13$^{\rm h}$04$^{\rm m}$.4−61°58′	−35						
RCW 75	−28		−29 (1)			2.3	

Table 1. continued

Object name	Hα km s^{-1}	H 109α km s^{-1}	CO km s^{-1}	Abs km s^{-1}	V_{syst} km s^{-1}	$d_\star$ kpc	$d_{adopted}$ kpc
306.315−0.361	(−18)	−16	−34/−21/−18 (1)	−19 (2)	−20		1.5
308.092−0.432		−17		−57/−13 (2)	−17		9.3
Hα13^{h}23.^{m}8−63°23′	−24						
					−25		1.7
Hα13^{h}25.^{m}6−63°31′	−25						
307.569−0.616		−40	−35/−11 (1)				
					−36		2.8
307.620−0.32	−38	−37	−44/−37 (1)				
308.647+0.579	−49	−50		−46 (4)		4.0	
= RCW 79							
309.057+0.186	−48	−47	−55/−38 (1)		−50		
309.905+0.373		−55	−57/−40 (1)	−58/−40 (2) −40 (4)			4.2
309.548−0.737	−47	−43	−52/−41 (1)	−51 (2)			
RCW78	−48					4.2	
CO 311.3−0.3			27 (3)				
310.796−0.408		33/(−57)	−50/ −24 (1)	−50 (2)	33		14.1
311.114−0.270		36	−56 (1)				
311.619−0.599		32	−50 (1)				
310.994+0.389	−50	−51	−55/−48/−39/−35 (1)				
= RCW 82							
311.288−0.021		−52	−39/−35 (1)		−51		3.4
Hα13^{h}57.^{m}5−62°2′	−50						
Hα13^{h}56.^{m}0−62°23′	−49					2.9	
311.197+0.752		−57		49 (2)			
311.489+0.368		−59	−59/−57/−48/−31 (1)	−56 (2) −53/−34 (4)	−60		5.6
311.627+0.270		−61	−52/−33/−14/0 (5)	−54/−49 (2)			
311.852−0.222		−55	−63/(−50)/−42 (1)				
311.497−0.483		−47	−49/−39/−25/−20 (1)				
311.894+0.100		−47	−54/−46	−52/−45 (2)			
				−40 to −60/−26/−3 (7)			
311.922+0.229		−45	−49/−13 (5)	−52/−45(2)	−47		7.5
				−40 to −60/−27/−4(7)			
312.112+0.314		−49	−48/(−35) (1)	−49 (2)			
312.953−0.449		−47	−47/−38/−17 (1)				
RCW 83	−31						
RCW 85	−31				−25	1.5	1.5
Hα14^{h}17.7^m−63°26′	−24						
313.446+0.176		−5	−50/−23 (1)	−4 (2)	−5		11.5
314.098+0.480		−67	−16/−12 (1)				
314.183+0.314		−62	−62/−43 (1)	−61 (12)			
314.228+0.437		−63	−57/−46 (1)	−61 (2)	−61		7.2
CO 315.0+0.0			−58 (8)				
316.156−0.492		−60	−61/−54/−50/−44 (1)				
CO 315.3−0.3			14 (3)				
					15		13.3
315.312−0.273		16	−49/−46/13 (1)				
316.393−0.356		3	−46 ? (1)	−47/−4	3		12.5
316.808−0.037	−36	−36	−40 (9) −41 (10)	−47/−37 (6)		3.6	
			−46/−39/−20 (5)	−53/−45/−3/ −21/−12/−3 (11)			
317.037+0.300	−42	−49	(−50)/−44 (1)	−48 (12)			
Hα14^{h}43.6^m−58°43′	−46				−44		3.6
317.291+0.268	−51	−51	−45 (1)				
Hα14^{h}45.7^m−59°33′	−46						
Hα14^{h}46.7^m−59°41′	−46						
317.598−0.363	−46	−38	−9/−5/−1 (1)				
317.988−0.759	−37	−37	(45/−23) (1)				

Table 1. continued

Object name	Hα km s^{-1}	H 109α km s^{-1}	CO km s^{-1}	Abs km s^{-1}	$V_{\rm syst}$ km s^{-1}	$d_\star$ kpc	$d_{\rm adopted}$ kpc
318.058−0.459		−31	−56/−48/12 (1)	−47 (2)	−34		10.4
318.911−0.181		−29	−42/−34/−23 (1)	−34 (2)			
318.058−0.459		37			30		15.4
CO 318.0−0.3			30				
319.157−0.423		−22	−39/−23/−20 (1)	−20 (2) −21 (6)	−20		11.5
319.380−0.025		−14	(−57)/−43/−19 (1)	(−46)/−20 (6)			
319.874+0.770		−38	−43/−42 (1)	−41			
320.153+0.780	−43	−36	−40 (9)	−40 (6)	−40		2.7
= RCW 87							
320.236+0.417	−31	−31	−32 (1)	−31 (2)	−31		2.1
= RCW 88							
320.109−0.510		−13	−55/−45 (1)				
320.317−0.208		−11		−11 (6)	−7		12.7
320.379+0.139		−3		−3 (2)			
320.706+0.197		−7					
320.252−0.332	−68	−68	(−75/−45) (1)	−13 (6)	−68		4.7
BBW 28802	−5						0.2
RCW 89 (SNR)	−48	−50 (13)		−60/−12/−4 (7)	−50	3.3	3.3
Hα[320.5−1.4]	−51						
321.038−0.519		−61	−81/−71/−61 (1)	−62 (2) −63 (6)	Note		
=RCW 91	−64				−60		
321.105−0.549		−56	−62/−58/−54 (1)				3.8
Hα$15^{\rm h}12.7^{\rm m}-58°17'$	−57						
322.153+0.613	−56	−52	−55 (9) −56/−35 (5)	−54/−40/−4 (6) −56/−32/−21 (7)	−55		
= RCW 92				−55 (12)			
321.710+1.157		−32			−31		11.3
322.407+0.221		−30					
324.120−0.954	−65	−67			−66		4.3

(1) Russeil & Castets (1998)
(2) Caswell & Haynes (1987)
(3) Grabelsky et al. (1988)
(4) Whiteoak & Gardner (1974)
(5) Whiteoak et al. (1982)
(6) Gardner & Whiteoak (1984)
(7) from profiles of Caswell et al. (1975)
(8) Israel et al. (1984)
(9) Gillespie et al. (1977) and Gillespie et al. (1979)
(10) White & Philips (1982)
(11) Goss et al. (1972)
(12) Caswell & Robinson (1974)
(13) Dopita et al. (1977)
(14) Brand et al. (1984)
(15) Brand (1986).

mixing of several HII regions due to their internal motions. Previously discussed by Georgelin et al. (1987), the star forming region $316.808-0.037$ exhibits a radio maximum corresponding to weak Hα emission. The mean velocity of the entire Hα emission is −36 km s^{-1} with a line width broader than usual. In fact, the Hα radial velocities of the different condensations are between −34 and −43 km s^{-1}, indicating significant internal motions. The star LSS 3280 (spectral type O9III) is very close to this HII region and likely participates in its excitation. Its distance is 3600 pc. Also RCW 91, associated with radio sources $321.038-0.519$ and $321.105-0.549$, has large internal motions. The different condensation velocities are between −59 and −67 km s^{-1} with broad line widths. Study of the young stellar content shows 19 stars with distances greater than 2 kpc, for which the mean distance is 3.4 ± 1.5 kpc. Note that Hα [320.5 − 1.4], excited by Pis 20 (d = 3.3 kpc; Turner 1996) has a more negative velocity, by about 10 km s^{-1}, than that found in 1987 (Georgelin et al. 1987).

Finally, 321.7+1.1 and 322.4+0.2 (mean velocity −31 km s^{-1}), which are not detected at Hα, are assumed to be at the far distance of 11.3 kpc.

4. Conclusion

Whatever the direction of the line of sight a diffuse local component is widely observed from Galactic longitude

301° to 323°. Linked to the local arm, this component is associated with the Coalsack and other dark clouds in the vicinity, and also to the OB Sco-Cen association which is at the origin of this negative interstellar medium velocity component ($-10 < V_{\rm lsr} < 0$ km s^{-1}) between $l = 295°$ and 341° (Crawford 1991). We thus choose a distance of 170 pc for this component.

Except for this diffuse component and the distant sources with positive velocities, the Hα emission produced by discrete and diffuse sources shows a rather intricate kinematic behaviour. Indeed, the velocity components exhibit a large range of variation difficult to interpret in terms of independent groups, particularly toward areas where the regions are likely exhibiting large internal motions, e.g. at $l = 305°$. In some zones (e.g. at $l = 320°$) a study with wider observing fields would be necessary to conclude.

We have tried to distinguish the different complexes met along the various lines of sight using the multiwavelength information. Some groups have velocities allowing no kinematic distance determination due to circular rotation departures.

In order to interpret the studied area in terms of the spiral structure we need to connect it with the adjacent zones observed in the Hα Survey. This study is in progress.

Acknowledgements. The authors are most grateful to J. Caplan for English translation.

References

Bok B.J., Bester M.J., Wade C.M., 1955, Harward reprint 416
Brand J., 1986, Ph. D. Thesis, University of Leiden
Brand J., Blitz L, 1993, A&A 275, 67
Brand J., van der Bij M.D.P., de Vries C.P., et al., 1984, A&A 139, 181
Bronfman L., Alvarez H., Cohen R.S., Thaddeus P., 1989, ApJS 71, 481
Caswell J.L., Robinson B.J., 1974, Aust. J. Phys. 27, 597
Caswell J.L., Robinson B.J., 1995, A&AS 111, 75
Caswell J.L., Haynes R.F., 1987, A&A 171, 261
Caswell J.L., Murray J.D., Roger R.S., Cole D.J., Cooke D.J., 1975, A&A 45, 239
Crawford I.A., 1991, A&A 247, 183
Crawford I.A., 1992, MNRAS 254, 264
Dame T.M., Ungerechts H., Cohen R.S., et al., 1987, ApJ 322, 706
Danks A.C., Wamsteker W., Shaver P.A., Retallack D.S., 1984, A&A 132, 301
Dopita M.A., Mathewson D.S., Ford V.L., 1977, ApJ 214, 179
Duncan A.R., Stewart R.T., Haynes R.F., Jones K.L., 1995, MNRAS 277, 36
Gardner F.F., Whiteoak J.B., 1984, MNRAS 210, 23
Georgelin Y.M., Boulesteix J., Georgelin Y.P., Laval A., Marcelin M., 1987, A&A 174, 257
Georgelin Y.M., Boulesteix J., Georgelin Y.P., le Coarer E., Marcelin M., 1988, A&A 205, 95
Georgelin Y.M., Amram P., Georgelin Y.P., et al., 1994, A&AS 108, 513
Georgelin Y.P., Georgelin Y.M., 1970, A&AS 3, 1
Gillespie A.R., Huggins P.J., Sollner T.C.L.G., et al., 1977, A&A 60, 221
Gillepsie A.R., White G.J., Watt G.D., 1979, MNRAS 186, 383
Goss W.M., Radhakrishnan V., Brooks J.W., Murray J.D., 1972, ApJS 24, 123
Grabelsky D.A., Cohen R.S., Bronfman L., Thaddeus P., 1988, ApJ 331, 181
Haynes R.F., Caswell J.L., Simons L.W.J., 1978, Aust. J. Phys. Astrophys. Suppl. 45, 1
Israel F.P., de Graaww Th., de Vries C.P., et al., 1984, A&A 134, 396
le Coarer E., Amram P., Boulesteix J., et al., 1992, A&A 257, 389 (Paper I)
Lynga, 1987, Catalogue of open cluster data, CDS, Strasbourg
Mc Carthy C., Miller E.W., 1973, AJ 78, 33
Nyman L.A., Bronfman L., Thaddeus P., 1989, A&A 216, 185
Reynolds R.J., 1979, ApJ 229, 942
Reynolds R.J., 1984, ApJ 282, 191
Reynolds R.J., 1987, ApJ 323, 118
Rodgers A.W., Campbell C.T., Whiteoak J.B., 1960, MNRAS 121, 103
Russeil D., 1997, A&A 319, 788
Russeil D., Castets A., 1998 (in preparation)
Seidensticker K.J., Schmidt Kaler Th., 1989, A&A 225, 192
Schmidt Kaler Th., 1983, Landolt-Borstein, New Series, Group Obs. 1, 100
Turner D.G., 1996, AJ 111, 828
Whiteoak J.B., Gardner F.F., 1974, A&A 37, 389
Whiteoak J.B., Otrupcek R.E., Rennie C.J., 1982, Proc. ASA 4, 434
White G.J., Philips J.P., 1982, Regions of Recent star formation. Reidel Dordrecht, p. 231